

Mathematical Modeling of Microscale Biology: Ion Pairing, Dielectric Decrement, and Born Energy in Glycosaminoglycan Brushes

William J Ceely,^{*} Marina Chugunova,[†] and Ali Nadim[‡]
*Institute of Mathematical Sciences
Claremont Graduate University*

James D Sterling[§]
*Henry E. Riggs School of Applied Life Sciences
Keck Graduate Institute*
(Dated: June 27, 2022)

Biological macromolecules including nucleic acids, proteins, and glycosaminoglycans are typically anionic and can span domains of up to hundreds of nanometers and even micron length scales. The structures exist in crowded environments that are dominated by weak multivalent electrostatic interactions that can be modeled using mean field continuum approaches that represent underlying molecular nanoscale biophysics. We develop such models for glycosaminoglycan brushes using both steady state modified Poisson-Boltzmann models and transient Poisson-Nernst-Planck models that incorporate important ion-specific (Hofmeister) effects. The results quantify how electroneutrality is attained through ion electrophoresis, dielectric decrement hydration forces, and ion-specific pairing. Brush-Salt interfacial profiles of the electrostatic potential as well as bound and unbound ions are characterized for imposed jump conditions across the interface. The models should be applicable to many intrinsically-disordered biophysical environments and are anticipated to provide insight into the design and development of therapeutics and drug-delivery vehicles to improve human health.

I. INTRODUCTION

Many biological structures are characterized by beds of intrinsically-disordered anionic biopolymers. In particular, nucleic acids, proteins, and extracellular glycosaminoglycans (GAGs) are polyelectrolytes that perform functions controlled by their hydration and their neutralization by cations and cationic residues of associated proteins. These anionic beds of slowly-diffusing macromolecules can be considered *fixed* in space over times scales of counterion neutralization phenomena. Although transient phenomena occur with molecular conformation changes, we can place the reference frame at the center of mass of the bed of the macromolecules to make analysis tractable. If the anionic bed is tethered to a tissue- or cell-surface, or a biopolymer is grafted to a surface, simplified structural models known as *brushes* can be defined and there is a long history of brush research in polymer and surface science [1–4].

Another set of simplified structural models of anionic biopolymer beds are spherical *biomolecular condensates*. Here, non-tethered anionic macromolecules interact with counterion atoms and molecules to form two co-existing liquid phases where a dense phase appears in the form of microscale spheres within a dilute phase. The discovery of biomolecular condensates (or *membraneless organelles*) has revolutionized our perspective of biological structure and function, as the formation of conden-

sates helps explain the acceleration of biochemical reaction rates and epigenetic control of biological processes that occur in both intracellular and extracellular domains [5, 6]. In polymer science, such condensates fall within the broader category of *coacervates* as described in the two recent review articles [7, 8].

Pathologies associated with cell surfaces, mucosal surfaces, and membraneless organelles can be recapitulated in laboratory studies of biological structures that can be approximated as brushes and biocondensates. Thus, in a relatively new approach to drug discovery, biomacromolecules can be designed and applied to control microscale biology for therapeutic benefit. Examples include well-known polysaccharides such as heparin and hyaluronic acid as well as more recent cationic-lipids used in mRNA vaccines [9], poly(acetyl, argyl) glucosamine (PAAG) for mucosal disorders [10], as well as cationic arginine-rich peptides for drug delivery applications [11].

In this paper, we develop a broadly-applicable mean-field mathematical model of anionic beds of macromolecules neutralized by cations focusing specifically on *GAG brushes* as a test case. The model aims to elucidate complexities of the biophysics of these molecularly-crowded environments where there is a delicate balance of weak multivalent electrostatic ion-pairing accompanied by release of water and ions upon binding. An ordinary differential equation (ODE) model is developed that depicts steady state electrostatic interactions of a GAG brush in a bulk salt solution taking into account spatial variation of the permittivity (*dielectric decrement*), which leads to ion Born Hydration energy gradients, and ion pairing between the salt and the GAG brush. This model is known as a modified Poisson-Boltzmann (MPB) model. We then introduce transient partial differential

* william.ceely@cgu.edu

† marina.chugunova@cgu.edu

‡ ali.nadim@cgu.edu

§ jim.sterling@kgi.edu

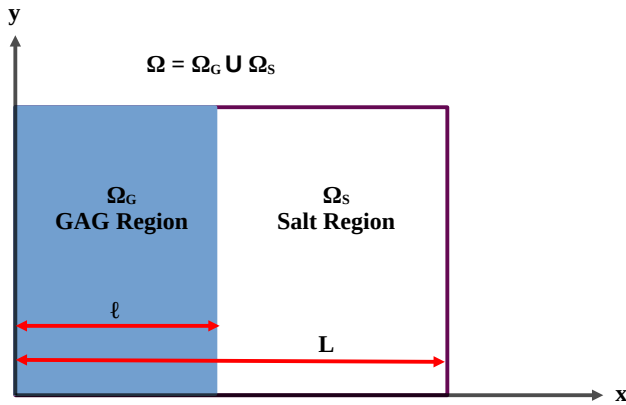


FIG. 1. Schematic of model depicting GAG brush region, $\Omega_G = \{0 \leq x \leq \ell\}$, Salt region, $\Omega_S = \{\ell \leq x \leq L\}$, and total domain, $\Omega = \Omega_G \cup \Omega_S$.

equations (PDEs) that include the flux and reaction rates of ions that react with counterions to form ion-pairs. The combination of the electrostatics equation and species transport equations are known as Poisson-Nernst-Planck (PNP) equations.

We begin with the derivations of two PB models using different assumptions for the variation of GAG brush-salt permittivity. We then compare our models to a previous model [12], which does not incorporate dielectric decrement or ion pairing, showing how electrostatic potential and ion concentration profiles match in the limit and we compare results from both models. We then consider molecular simulation data [13], which show that dielectric decrement and ion pairing lead to Born energy and a binding energy, respectively. We show how to relate the binding energy to our dissociation constant and compare predictions from our model to the simulation data. We then consider extensions to the model that include two counterions and show that the PNP models are stable and relax to the expected PB steady-states. Finally, we end with a discussion of our model applicability, its shortcomings, and future directions of this work.

II. THE STEADY-STATE MODEL

To derive a mathematical model to describe the electrostatics in Figure 1, we begin, as normal, with the differential form of Gauss's law:

$$\nabla \cdot (\varepsilon \mathbf{E}) = \rho, \quad \text{in } \Omega, \quad (1)$$

where \mathbf{E} is the electric field, ρ is the total charge density, and ε is the permittivity of the medium. Assuming electrostatic conditions or that the magnetic field variation with time is negligible, the curl of the electric field can be assumed zero: $\nabla \times \mathbf{E} \approx \mathbf{0}$, so that we can define a relationship between the electric field and the potential

as:

$$\mathbf{E} = -\nabla\phi, \quad \text{in } \Omega. \quad (2)$$

Substituting (2) into (1), we arrive at:

$$-\nabla \cdot (\varepsilon \nabla\phi) = \rho, \quad \text{in } \Omega. \quad (3)$$

The total charge density is related to the unbound concentration of the ions present:

$$\rho = \sum_i z_i N_A e [C_i], \quad (4)$$

where z_i is the valence and $[C_i]$ is the unbound concentration of ion i , respectively, N_A is Avogadro's constant, and e is the elementary charge. We make the simplifying assumption that the variation in potential and ion concentrations is only present in the x -direction, which reduces our model to a single 2nd order ODE.

$$-\frac{d}{dx} \left(\varepsilon \frac{d\phi}{dx} \right) = \sum_i z_i N_A e [C_i], \quad \text{in } \Omega. \quad (5)$$

Finally, we focus on a negatively charged GAG in a monovalent salt solution and thus $z_i = \pm 1$.

$$-\frac{d}{dx} \left(\varepsilon \frac{d\phi}{dx} \right) = N_A e ([C^+] - [A^-] - [G^-]), \quad \text{in } \Omega, \quad (6)$$

where $[C^+]$ represents the cation concentration (such as Na^+ or K^+), $[A^-]$ represents the anion concentration (such as Cl^-), and $[G^-]$ represents the unbound fixed GAG concentration.

Previous models [12] assume a constant permittivity throughout the whole domain. However, molecular simulations [13] show a decrease in the permittivity (dielectric decrement) within the GAG region. In what follows, we continue to develop our model using two different assumptions about how the permittivity and total concentration of the GAG vary throughout the domain. To this end, we incorporate a Born energy term [14] to account for this varying permittivity. The Born energy is given by

$$U_i = \frac{z_i^2 e^2}{8\pi \varepsilon r_i}, \quad (7)$$

where r_i is the Born radius of ion i . This is an effective radius and not a physically measured ion radius.

We also take into account ion pairing (the ability for the cation to bind to the GAG ions). In a reversible reaction, at equilibrium we must have $k_1 [G^-][C^+] = k_{-1} [GC]$, which leads to:

$$[GC] = \frac{[C^+]}{(k_{-1}/k_1)} [G^-] = \frac{[C^+]}{K_1} [G^-]. \quad (8)$$

Here $[GC]$ is the concentration of the GAG and the cation that are bound together, k_1 is the forward reaction rate

constant at which the GAG and the cation bind together, k_{-1} is the backward reaction rate constant at which the bound GAG and cation break apart, and

$$K_1 \equiv \frac{k_{-1}}{k_1}, \quad (9)$$

is known as the dissociation constant and has units of concentration.

The total GAG concentration, $[G^-]_0$, is the sum of the unbound GAG concentration, $[G^-]$, and the concentration of GAG that is bound to the cation, $[GC]$. Therefore, $[G^-]_0 = [G^-] + [GC] = [G^-] (1 + [C^+]/K_1)$, resulting in:

$$[G^-] = \frac{[G^-]_0}{(1 + [C^+]/K_1)}. \quad (10)$$

A. Piecewise Constant Permittivity and Total GAG Concentration

The simplest assumption that we can make for the varying permittivity and total GAG concentration is to assume piecewise constant values for both. This allows us to break the problem into two separate domains where the permittivity and the total GAG concentration are both constant.

Let

$$\varepsilon = \varepsilon_0 \varepsilon_r \varepsilon_x, \quad (11)$$

where ε_0 is the vacuum permittivity, ε_r is the dielectric constant of a reference medium, and

$$\varepsilon_x = \begin{cases} \varepsilon_S, & \text{in } \Omega_S \\ \varepsilon_G, & \text{in } \Omega_G \end{cases}, \quad (12)$$

are constant scaling factors to the permittivity in the Salt and GAG regions.

In the Salt region, the total GAG concentration is taken to be zero. Thus, we can represent the ODE of equation (7) as:

$$-\varepsilon_0 \varepsilon_r \varepsilon_S \frac{d^2 \phi}{dx^2} = N_A e ([C^+] - [A^-]) \quad \text{in } \Omega_S. \quad (13)$$

We scale all concentrations with some concentration, C_0 . Possible choices for C_0 are the bulk concentration of the salt or the total GAG concentration. Define the dimensionless concentrations as

$$c \equiv \frac{[C^+]}{C_0}, \quad a \equiv \frac{[A^-]}{C_0}. \quad (14)$$

Scale the electric potential, ϕ , with the thermal voltage

$$\frac{k_B T}{e} = \frac{N_A k_B T}{N_A e} = \frac{RT}{F}, \quad (15)$$

where k_B , T , R , and F are Boltzmann constant, absolute temperature, gas constant, and Faraday constant, respectively. Define the dimensionless potential as

$$y \equiv \frac{\phi}{(RT/F)}. \quad (16)$$

Substituting (14), (15), and (16) into (13) and dividing both sides by F yields:

$$-\frac{\varepsilon_0 \varepsilon_r \varepsilon_S RT}{F^2 C_0} \frac{d^2 y}{dx^2} = c - a. \quad (17)$$

To nondimensionalize lengths, we define a modified Debye length, λ_D as

$$\lambda_D^2 = \frac{\varepsilon_0 \varepsilon_r RT}{F^2 C_0}, \quad (18)$$

and scale x , ℓ , and L by λ_D . That is,

$$\hat{x} = \frac{x}{\lambda_D}, \quad \hat{\ell} = \frac{\ell}{\lambda_D}, \quad \hat{L} = \frac{L}{\lambda_D}. \quad (19)$$

Our dimensionless ODE in the salt region becomes:

$$-\frac{d^2 y}{d\hat{x}^2} = \frac{1}{\varepsilon_S} (c - a) \quad \text{in } \Omega_S. \quad (20)$$

In crowded macromolecular environments, details of hydration can substantially impact ion motion and partitioning. Thus, assuming that ions partition according to Boltzmann distributions that combine electrostatic energy with Born hydration energy [15], we can write:

$$c = \bar{c} \exp(-y - \hat{u}_c/\varepsilon_S), \quad (21)$$

$$a = \bar{a} \exp(y - \hat{u}_a/\varepsilon_S), \quad (22)$$

where $\hat{u}_c = e^2/8\pi k_B T \varepsilon_0 \varepsilon_r r_c$ and $\hat{u}_a = e^2/8\pi k_B T \varepsilon_0 \varepsilon_r r_a$ are the dimensionless Born energies in the reference medium with dielectric constant ε_r for the cation and anion, respectively. The dimensionless PB equation in the salt region thus takes the explicit form:

$$-\frac{d^2 y}{d\hat{x}^2} = \frac{1}{\varepsilon_S} [\bar{c} \exp(-y - \hat{u}_c/\varepsilon_S) - \bar{a} \exp(y - \hat{u}_a/\varepsilon_S)] \quad \text{in } \Omega_S. \quad (23)$$

Since the potential is relative, we need to define the zero reference. We choose to define the reference potential where electroneutrality is locally met. That is, take $d^2 y/d\hat{x}^2 \equiv 0$ where $y = 0$ in Ω_S , so that:

$$0 = \bar{c} \exp(-\hat{u}_c/\varepsilon_S) - \bar{a} \exp(-\hat{u}_a/\varepsilon_S) \quad (24)$$

This can be written as $\tilde{c} = \tilde{a}$, where $\tilde{c} = \bar{c} \exp(-\hat{u}_c/\varepsilon_S)$ and $\tilde{a} = \bar{a} \exp(-\hat{u}_a/\varepsilon_S)$ are rescaled dimensionless concentrations in the bulk salt solution.

The final version of the governing equations, known as the Born-energy augmented Poisson-Boltzmann equation [16], reduce to the following. In the Salt region we have:

$$-\frac{d^2 y}{d\hat{x}^2} = \frac{\tilde{c}}{\varepsilon_S} [e^{-y} - e^y] \quad \text{in } \Omega_S. \quad (25)$$

In the GAG region, the total GAG concentration, $[G^-]_0$, is taken to be constant, whereby:

$$-\varepsilon_0\varepsilon_r\varepsilon_G \frac{d^2\phi}{dx^2} = N_A e \left([C^+] - [A^-] - \frac{[G^-]_0}{(1 + [C^+]/K_1)} \right) \quad \text{in } \Omega_G. \quad (26)$$

Using the same scaling parameters (C_0 , RT/F , λ_D) from

$$-\frac{d^2y}{d\hat{x}^2} = \frac{\tilde{c}}{\varepsilon_G} \left\{ \exp\left(-y - \hat{u}_c \left[\frac{1}{\varepsilon_G} - \frac{1}{\varepsilon_S}\right]\right) - \exp\left(y - \hat{u}_a \left[\frac{1}{\varepsilon_G} - \frac{1}{\varepsilon_S}\right]\right) \right\} - \frac{1}{\varepsilon_G} \left\{ \frac{\bar{g}}{1 + (\tilde{c}/\tilde{K}_1) \exp\left(-y - \hat{u}_c \left[\frac{1}{\varepsilon_G} - \frac{1}{\varepsilon_S}\right]\right)} \right\} \quad \text{in } \Omega_G. \quad (30)$$

The value of the dimensionless potential, y , that makes the right-hand side zero is known as the Donnan potential, y_D .

Thus, the model assuming piecewise constant permittivity and total GAG concentration is complete with equations (25) and (30) along with the boundary conditions:

$$y(\hat{\ell}^-) = y(\hat{\ell}^+), \quad (31a)$$

$$\varepsilon_G \frac{d}{d\hat{x}} y(\hat{\ell}^-) = \varepsilon_S \frac{d}{d\hat{x}} y(\hat{\ell}^+). \quad (31b)$$

$$-\frac{d}{d\hat{x}} y(0) = \hat{\sigma}_2. \quad (31c)$$

$$\frac{d}{d\hat{x}} y(\hat{L}) = \hat{\sigma}_1. \quad (31d)$$

$$-\varepsilon_1(\hat{x}) \frac{d^2y}{d\hat{x}^2} - \frac{d\varepsilon_1(\hat{x})}{d\hat{x}} \frac{dy}{d\hat{x}} = \bar{c} \exp\left(-y - \frac{\hat{u}_c}{\varepsilon_1(\hat{x})}\right) - \bar{a} \exp\left(y - \frac{\hat{u}_a}{\varepsilon_1(\hat{x})}\right) - \frac{\bar{g}(\hat{x})}{1 + \bar{c}/\tilde{K}_1 \exp\left(-y - \hat{u}_c/\varepsilon_1(\hat{x})\right)} \quad \text{in } \Omega, \quad (33)$$

with boundary conditions:

$$-\frac{d}{d\hat{x}} y(0) = \hat{\sigma}_2, \quad (34a)$$

the salt region derivation we obtain:

$$-\frac{d^2y}{d\hat{x}^2} = \frac{1}{\varepsilon_G} \left[c - a - \frac{\bar{g}}{1 + \bar{c}/\tilde{K}_1} \right] \quad \text{in } \Omega_G, \quad (27)$$

where $\bar{g} = [G^-]_0/C_0$ and $\tilde{K}_1 = K_1/C_0$. Again, assuming Boltzmann distributions combined with Born energy for the mobile ions:

$$c = \tilde{c} \exp\left(-y - \hat{u}_c \left[\frac{1}{\varepsilon_G} - \frac{1}{\varepsilon_S}\right]\right), \quad (28)$$

$$a = \tilde{c} \exp\left(y - \hat{u}_a \left[\frac{1}{\varepsilon_G} - \frac{1}{\varepsilon_S}\right]\right). \quad (29)$$

The final version of the ODE in the GAG region is:

The first two conditions equate the potential and positive and negative surface charge densities at the interface. For electroneutrality to hold overall, we must have $\hat{\sigma}_1 = -\hat{\sigma}_2$. These are the surface charge densities at the two boundaries.

B. Smoothly Varying Permittivity and Total GAG Concentration

Perhaps a more accurate assumption for the varying permittivity and total GAG concentration is to take them to vary smoothly with respect to x rather than being discontinuous at the interface. The same PB equation thus holds throughout the domain:

$$-\varepsilon_0\varepsilon_r \frac{d}{dx} \left(\varepsilon_1(x) \frac{d\phi}{dx} \right) = N_A e \left([C^+] - [A^-] - [G^-] \right). \quad (32)$$

Using the same scaling parameters (C_0 , RT/F , λ_D , \hat{u}_c , and \hat{u}_a) from section II A, the dimensionless ODE model $-\varepsilon_1(\hat{x})y'(\hat{x})' = c - a - g$ becomes:

$$\frac{d}{d\hat{x}} y(\hat{L}) = \hat{\sigma}_1. \quad (34b)$$

To complete the model, we need to define the smooth functions $\varepsilon_1(\hat{x})$ and $\bar{g}(\hat{x})$. A convenient choice for a smooth function is the hyperbolic tangent. Let

$$f(\hat{x}) = \frac{1}{2} \left[\tanh \left(\frac{1 - \hat{x}/\hat{\ell}}{\alpha} \right) + 1 \right], \quad (35)$$

which has the first derivative

$$f'(\hat{x}) = -\frac{1}{2\hat{\ell}\alpha} \left[\operatorname{sech} \left(\frac{1 - \hat{x}/\hat{\ell}}{\alpha} \right) + 1 \right]^2. \quad (36)$$

The transition is centered at $\hat{x} = \hat{\ell}$, and $\alpha > 0$ controls the transition length. We then define

$$\bar{g}(\hat{x}) \equiv g_0 f(\hat{x}), \quad (37)$$

$$\varepsilon_1(\hat{x}) \equiv (\varepsilon_G - \varepsilon_S) f(\hat{x}) + \varepsilon_S, \quad (38)$$

$$\frac{d\varepsilon_1(\hat{x})}{dx} \equiv (\varepsilon_G - \varepsilon_S) f'(\hat{x}). \quad (39)$$

We can express \bar{a} in terms of \bar{c} by defining the first and second derivative of y to be zero when $y = 0$, noting that $\varepsilon_1 \approx \varepsilon_S$ and $\bar{g} \approx 0$ in this case. With this we see that

$$\bar{a} = \bar{c} \exp \left(\frac{\hat{u}_a - \hat{u}_c}{\varepsilon_S} \right). \quad (40)$$

We argue that this model is equivalent to the model in §II A in the limit. With the proposed smooth function, for $\alpha \ll 1$, the permittivity and total GAG concentration are essentially piecewise constant except for near the interface ($\hat{x} \approx \hat{\ell}$). So the model in §II A is an approximation to this model away from the interface. Further, we also note that as $\alpha \rightarrow 0$,

$$f(\hat{x}) \rightarrow \begin{cases} 1, & \text{in } \Omega_G \\ 0, & \text{in } \Omega_S \end{cases}, \quad (41)$$

that is, $f(\hat{x})$ approaches a piecewise constant function, and this version of the model approaches that of section II A.

III. PREVIOUS VOLUME CHARGE MODEL: GAG BRUSH NEAR A CHARGED SURFACE

A. Brief Description of the Model

Dean et al. [12] provide three mathematical PB models to describe the electrostatic interactions of a negatively charged chondroitin sulfate GAG in a bulk NaCl salt solution. The basic form of the models is

$$\nabla^2 \Phi = \frac{2FC_0}{\varepsilon_w} \sinh \left(\frac{F\Phi}{RT} \right) - \frac{\rho_{\text{fix}}}{\varepsilon_w}, \quad (42)$$

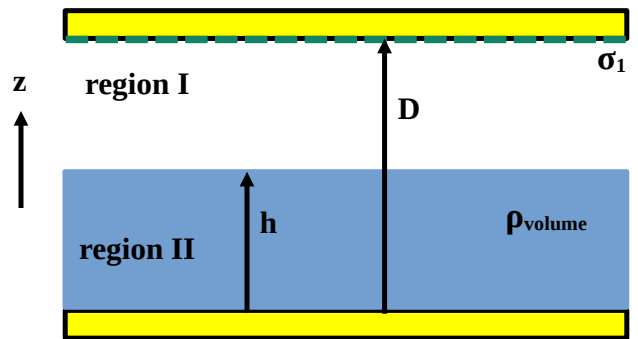


FIG. 2. Schematic of constant volume charge model depicting GAG brush with constant volume charge density, ρ_{volume} , in region II of height, h , bulk salt in region I extending from $h \leq z \leq D$, and surface charge density, σ_1 . Recreated from [12].

where C_0 is the bath concentration of NaCl, ρ_{fix} is a fixed charge density term and ε_w is the permittivity of the bulk solution.

The volume charge model in Figure 2 approximates the GAG brush as a fixed uniform volume charge density of height, h . Inside the GAG brush region, the ODE has the form

$$\nabla^2 \Phi = \frac{2FC_0}{\varepsilon_w} \sinh \left(\frac{F\Phi}{RT} \right) - \frac{\rho_{\text{volume}}}{\varepsilon_w}, \quad (43)$$

and in the salt region, the ODE has the form

$$\nabla^2 \Phi = \frac{2FC_0}{\varepsilon_w} \sinh \left(\frac{F\Phi}{RT} \right). \quad (44)$$

The boundary conditions are given as

$$\frac{\partial}{\partial z} \Phi(0) = 0, \quad (45a)$$

$$\frac{\partial}{\partial z} \Phi(D) = \frac{\sigma_1}{\varepsilon_w}, \quad (45b)$$

$$\Phi(h^-) = \Phi(h^+), \quad (45c)$$

$$\frac{\partial}{\partial z} \Phi(h^-) = \frac{\partial}{\partial z} \Phi(h^+). \quad (45d)$$

B. Relationship Between Models

The models in [12] assume a constant permittivity throughout both the salt and GAG regions. In our model, this would imply $\varepsilon_S = \varepsilon_G = 1$ and thus $\varepsilon_w = \varepsilon_0 \varepsilon_r$. Nondimensionalizing the ODEs, using the same scaling parameters from our model, and replacing z with x :

$$\frac{d^2 y}{dx^2} = 2\bar{c} \sinh(y) = \bar{c} [e^y - e^{-y}] \quad \text{in I,} \quad (46)$$

TABLE I. Parameters from [12].

Parameters	Volume Model
σ_1 (C/m ²)	-0.015
σ_2 (C/m ²)	0
Q (C)	-8.00×10^{-18}
s (nm)	6.5
h (nm)	20
D (nm)	30
ρ_{volume} (C/m ³)	$Q/(s^2h)$
T (K)	298
ε_w (C ² /N·m ²)	6.92×10^{-10}
C_0 (M)	0.01, 0.1, 1.0

$$\frac{d^2y}{dx^2} = \bar{c} [e^{-y} - e^{-y}] - \frac{\rho_{\text{volume}}}{FC_0} \quad \text{in II.} \quad (47)$$

These are similar to our model in equations (25) and (30), with two important differences. The first is that [12] does not include a Born energy term. However, because the permittivity is assumed constant, the Born energy would also be constant. Therefore, it could be lumped into the dimensionless concentration \bar{c} , which matches our \tilde{c} . The second difference is that [12] ignores any ion pairing. In other words, the total GAG concentration is equal to the unbound GAG concentration. If we allow the dissociation constant to approach ∞ , then $[G^-] \rightarrow -\rho_{\text{volume}}$, and we see that our model approaches the model in [12] in the limit.

Table I summarizes the parameters used in [12]. Table II summarizes the input parameters needed for our model described in Section II A and how they relate to the values in Table I. Note that since the permittivity is constant, the terms $\hat{u}_c [1/\varepsilon_G - 1/\varepsilon_S]$ and $\hat{u}_a [1/\varepsilon_G - 1/\varepsilon_S]$ from equation (30) are zero and not needed.

C. Comparison of Results

Using the model equations from [12] (summarized in equations (44)–(45d)), with the parameters summarized in Table I, we replicated the predicted profiles for potential, ϕ , and both the cation and anion concentration. We then used our model from Section II A, with the parameters summarized in Table II to generate the same profiles. The results are shown in Figure 3, with the solid colored lines representing the predictions from the model in [12] and the dashed/dotted lines representing the predictions from the model in Section II A. As can be seen, the predictions are in perfect agreement, further showing that in the limit, our model approaches the volume charge model in [12].

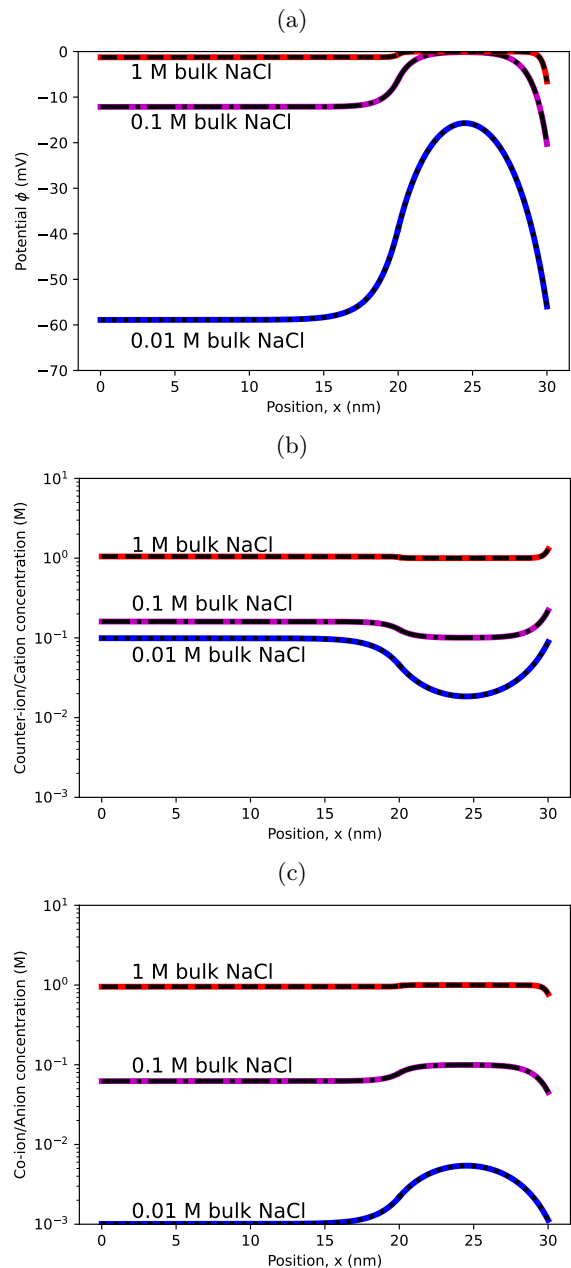


FIG. 3. (a) Potential, ϕ (mV), (b) cation concentration (M), and (c) anion concentration (M) using parameters from Tables I and II for $C_0 = 0.01$ M, 0.1 M, and 1.0 M. Solid colored lines represent the output using the model from [12] and dashed/dotted lines represent the output using the model from Section II A. Vertical axis scale chosen to match figures in [12].

IV. PREVIOUS MOLECULAR DYNAMICS SIMULATIONS: GAG BRUSH-SALT INTERFACE

A. Brief Description of Molecular Simulations

Sterling et al. [13] performed all-atom molecular dynamics nanoscale simulations of hyaluronic acid and hep-

TABLE II. Input Parameters to Piecewise Constant Permittivity and Total GAG Concentration Model.

Parameter	Notes	Value for $C_0 = 0.01$	Value for $C_0 = 0.1$	Value for $C_0 = 1$
ε_r	$\varepsilon_0/\varepsilon_w$	78.155	78.155	78.155
ε_S	Constant ε_w	1	1	1
ε_G	Constant ε_w	1	1	1
$\hat{\ell}$	h/λ_D	4.660	14.737	46.603
\hat{L}	D/λ_D	6.990	22.106	69.904
\tilde{K}_1	No Binding	10^{16}	10^{16}	10^{16}
\tilde{c}	C_0/C_0	1	1	1
\bar{g}	$\frac{-\rho_{\text{volume}}}{FC_0}$	9.812	9.812×10^{-1}	9.812×10^{-2}
$\hat{\sigma}_1$	$\frac{\sigma_1 F \lambda_D}{\varepsilon_w RT}$	-3.623	-1.146	-0.362
$\hat{\sigma}_2$	$\frac{-\sigma_2 F \lambda_D}{\varepsilon_w RT}$	0	0	0

arin GAG brushes in NaCl and KCl solutions. The results of the simulation are reported for the average brush values, represented by subscript b relative to values in the bulk salt layer denoted by subscript o including the Donnan potential, the dielectric decrement (variation of the permittivity), Born energy and the total concentrations of the ions. Thus, a Born-modified Boltzmann partitioning with ion-pair binding is proposed as:

$$c_{i,b} = c_{i,o} \exp \left(-\frac{q_i \varphi_b}{k_B T} - \frac{-\Delta G_i^s}{k_B T} \frac{\varepsilon_w}{\varepsilon_w - 1} \left[\frac{1}{\varepsilon_b} - \frac{1}{\varepsilon_o} \right] - \frac{\Delta \mu_i}{k_B T} \right), \quad (48)$$

where the first term represents the ion charge q_i in Donnan potential φ_b , the second term is the Born energy term, the third term represents the ion-pair binding free energy between ion atoms and brush anionic charges.

B. Relationship Between Simulation Data and Model

In [13], the simulation models consisted of a bulk solution occupying $z = -240\text{\AA}$ to 240\AA and GAG brushes of varying lengths, 2ℓ , centered at $z = 0$. Our model only considers the positive half of this domain $x = 0$ to 240\AA with the GAG brush occupying $x = 0$ to ℓ \AA. With zero-

gradient boundary conditions at 0 and ℓ , we model the interface between an infinite brush and infinite salt layer. The conditions relating quantities far from the interface represent so-called *jump conditions* that are analogous to the Rankine-Hugoniot conditions that are imposed across shock wave interfaces.

In the results from [13], total concentrations are used instead of those of the unbound charged ions, and a cation binding energy term is introduced. Modifying equation (30) to incorporate the binding energy and use total concentrations:

$$-\frac{d^2 y}{dx^2} = \frac{\tilde{c}}{\varepsilon_G} \left\{ \exp \left(-y - \hat{u}_c \left[\frac{1}{\varepsilon_G} - \frac{1}{\varepsilon_S} \right] - \frac{\Delta \mu}{k_B T} \right) - \exp \left(y - \hat{u}_a \left[\frac{1}{\varepsilon_G} - \frac{1}{\varepsilon_S} \right] \right) \right\} - \frac{\bar{g}}{\varepsilon_G}. \quad (49)$$

When $y = y_D$,

$$\bar{g} = \tilde{c} \left\{ \exp \left(-y_D - \hat{u}_c \left[\frac{1}{\varepsilon_G} - \frac{1}{\varepsilon_S} \right] - \frac{\Delta \mu}{k_B T} \right) - \exp \left(y_D - \hat{u}_a \left[\frac{1}{\varepsilon_G} - \frac{1}{\varepsilon_S} \right] \right) \right\}. \quad (50)$$

To find a relationship between the binding energy and the dissociation constant, substitute this into (30) with $y = y_D$ and solve for \tilde{K}_1 :

$$\tilde{K}_1 = \frac{\tilde{c} \{ \exp(-y_D - \hat{u}_c [1/\varepsilon_G - 1/\varepsilon_S]) - \exp(y_D - \hat{u}_a [1/\varepsilon_G - 1/\varepsilon_S]) \}}{\exp(-\Delta \mu / k_B T) - 1}. \quad (51)$$

The above relationships are only valid at the Donnan potential, to compute the binding energy for any potential, set the right-hand sides of (30) and (49) equal and solve

for $\exp(-\Delta \mu / (k_B T))$:

$$\exp \left(-\frac{\Delta \mu}{k_B T} \right) = 1 + \frac{\bar{g}}{\tilde{K}_1 + \tilde{c} \exp \left(-y - \hat{u}_c \left[\frac{1}{\varepsilon_G} - \frac{1}{\varepsilon_S} \right] \right)}. \quad (52)$$

Similarly, using equation (33) instead of (30), and noting that $\varepsilon_1(\hat{x}) = \varepsilon_G$ deep in the brush where the Donnan potential occurs, we find the relationships to be:

$$\tilde{K}_1 = \frac{\bar{c} \exp\left(-y_D - \frac{\hat{u}_c}{\varepsilon_G}\right) - \bar{a} \exp\left(y_D - \frac{\hat{u}_a}{\varepsilon_G}\right)}{\exp\left(-\frac{\Delta\mu}{k_B T}\right) - 1}, \quad (53)$$

or

$$\exp\left(-\frac{\Delta\mu}{k_B T}\right) = 1 + \frac{\bar{g}}{\tilde{K}_1 + \bar{c} \exp\left(-y - \frac{\hat{u}_c}{\varepsilon_1(\hat{x})}\right)}. \quad (54)$$

This can be used to compute the total cation concentration in addition to the unbound concentration.

C. Comparison of Results

Table III summarizes the parameters needed from [13] to generate the input parameters to the model in Section II B. The input parameters are listed in Table IV. Based on the literature, we expected the Born radius for Chloride to be 2.26 Å [17]. However, by using this value in our model, we found that Chloride would not be excluded from the brush as in the molecular simulation results. This led to a negative concentration of unbound GAG ions, a negative dissociation constant, and/or the inability to match the Donnan potential. By reducing the Born radius for Chloride by a factor of 10, our model was able to overcome these issues. Table IV shows the values of \hat{u}_a , \tilde{K}_1 , and \bar{a} based on both the expected Born radius and the actual value of 0.226 Å used in our model.

The value of α to control the transition length of the permittivity and total GAG concentration functions was qualitatively varied until the results in Table V and the total charge density curves in Figure 7(c) were in agreement with the corresponding data in [13].

As seen in Table V, our model predictions are well within the standard deviations from the molecular simulation results. All of our predicted energy values are within 0.014 of the average values obtained from the molecular simulations.

Plots of the predicted dimensionless potential, unbound charge density and total charge density curves can be found in Figures 4–7. For Figures 5 and 7 representing brushes with a potassium cation, the net charge density curves exhibit a double-double layer of negative charge just outside of the brush edge and positive charge just inside of the brush edge. Observing the electrostatic potential, we see the same trend as expected in a dilute-limit where dielectric decrement effects are negligible: a negative unbound charge density at an x -location corresponds to a positive second derivative in the electrostatic potential, while a positive unbound charge density corresponds to a negative second derivative in the electrostatic

potential. The molecular simulation data in [13] exhibited the opposite trend, positive charge just outside of the brush and negative charge just inside of the brush. It is unknown at this time why this discrepancy exists, but this is the only substantial difference between our model predictions and the molecular simulation data.

In contrast to the GAG brush results for the potassium cation, the net charge density curves in Figures 4 and 6 in the presence of a sodium cation show more complex structure. The brushes exhibit a negative charge inside the edge of brush, then a positive charge in the transition region and a negative charge on the outside edge of the brush. This corresponds to an electrostatic potential 2nd-derivative that is positive-negative-positive meaning there is a substantial *overshoot* of the potential rather than a smooth transition in the potential curve.

V. EXTENDING THE MODEL

The model as derived above focused on a monovalent salt solution consisting of one cation and one anion. This can be expanded to incorporate a second cation by modifying equation (6) to be

$$-\frac{d}{dx} \left(\varepsilon \frac{d\phi}{dx} \right) = N_A e \left([C_1^+] + [C_2^+] - [A^-] - [G^-] \right), \quad \text{in } \Omega, \quad (55)$$

where $[C_1^+]$ represents the cation 1 concentration and $[C_2^+]$ represents the cation 2 concentration. There are now two ion pairs, which leads to the modified equation (8) as

$$[GC_1] = \frac{[C_1^+]}{K_1} [G^-], \quad [GC_2] = \frac{[C_2^+]}{K_2} [G^-], \quad (56)$$

where K_1 and K_2 are the dissociation constants for cations 1 and 2, respectively.

The total GAG concentration, $[G^-]_0$, is now the sum of the unbound GAG concentration, $[G^-]$, and the concentrations of the two bound ion pairs, $[GC_1]$ and $[GC_2]$, i.e., $[G^-]_0 = [G^-] + [GC_1] + [GC_2]$. From this, we infer that:

$$[G^-] = \frac{[G^-]_0}{1 + [C_1^+]/K_1 + [C_2^+]/K_2}. \quad (57)$$

A. Piecewise Constant Model

Following the same procedure and definitions from section II A, we arrive at the modified ODE in the Salt region

$$-\frac{d^2 y}{d\hat{x}^2} = \frac{1}{\varepsilon_S} \left[\tilde{c}_1 e^{-y} + \tilde{c}_2 e^{-y} - (\tilde{c}_1 + \tilde{c}_2) e^y \right] \quad \text{in } \Omega_S. \quad (58)$$

Similarly, the modified ODE in the GAG region is

TABLE III. Parameters from [13].

GAG	Salt	Bulk Salt Conc. (M)	GAG Conc. (M)	Polymer Length (Å)	ε_b	ε_o	T (K)
Hyaluronan	NaCl	0.28	0.51	129.7	50.7	60.4	310.15
	KCl	0.28	0.49	135.8	51.2	61.8	310.15
Heparin	NaCl	0.27	2.78	119.3	37.5	59.1	310.15
	KCl	0.26	2.93	113.2	37.9	60.5	310.15

TABLE IV. Input Parameters to Smoothly Varying Permittivity and Total GAG Concentration Model.

Parameter	Notes	Hyaluronan NaCl	Hyaluronan KCl	Heparin NaCl	Heparin KCl
ε_r	Dilute Water, ε_w	78.155	78.155	78.155	78.155
$\varepsilon_1(\hat{L}) = \varepsilon_S$	$\varepsilon_o/\varepsilon_r$	0.773	0.791	0.756	0.774
$\varepsilon_1(0) = \varepsilon_G$	$\varepsilon_b/\varepsilon_r$	0.649	0.655	0.480	0.485
$\hat{\ell}$	Polymer Length/ $2/\lambda_D$	7.838	8.206	7.079	6.592
\hat{L}	$240\text{Å}/\lambda_D$	29.007	29.007	28.484	27.951
r_c (Å)	[17]	1.62	1.95	1.62	1.95
\hat{u}_C	Based on r_c	2.128	1.768	2.128	1.768
r_a (Å)	Expected Value[17]	2.26	2.26	2.26	2.26
	Used Value	0.226	0.226	0.226	0.226
\hat{u}_a	Based on Expected r_a	1.525	1.525	1.525	1.525
	Based on Used r_a	15.251	15.251	15.251	15.251
C_0	Salt Concentration	0.28	0.28	0.27	0.26
\tilde{K}_1	Expected Value, Eqn (53)	-0.115	-0.192	7.246×10^{-3}	-6.310×10^{-3}
	Used Value	0.172	0.114	1.337×10^{-2}	8.735×10^{-4}
\tilde{c}	Salt Concentration/ C_0	1	1	1	1
\bar{c}	$\tilde{c} \exp(\hat{u}_c/\varepsilon_S)$	15.692	9.350	16.671	9.810
\bar{a}	$\tilde{c} \exp[(\hat{u}_a - \hat{u}_c)/\varepsilon_S]$	7.196	6.881	7.515	7.172
	Used Value	3.721×10^8	2.380×10^8	5.744×10^8	3.602×10^8
g_0	GAG Concentration/ C_0	1.821	1.75	10.297	11.269
$\hat{\sigma}_1$	–	0	0	0	0
$\hat{\sigma}_2$	–	0	0	0	0
α	Expected Value	$\ll 1$	$\ll 1$	$\ll 1$	$\ll 1$
	Used Value	0.1	0.1	0.1	0.1

$$\begin{aligned}
-\frac{d^2y}{dx^2} = & \frac{1}{\varepsilon_G} \left\{ \tilde{c}_1 \exp\left(-y - \hat{u}_{c1} \left[\frac{1}{\varepsilon_G} - \frac{1}{\varepsilon_S}\right]\right) + \tilde{c}_2 \exp\left(-y - \hat{u}_{c2} \left[\frac{1}{\varepsilon_G} - \frac{1}{\varepsilon_S}\right]\right) \right. \\
& \left. - (\tilde{c}_1 + \tilde{c}_2) \exp\left(y - \hat{u}_a \left[\frac{1}{\varepsilon_G} - \frac{1}{\varepsilon_S}\right]\right) \right\} \\
& - \frac{1}{\varepsilon_G} \left\{ \frac{\bar{g}}{1 + \frac{\tilde{c}_1}{K_1} \exp\left(-y - \hat{u}_{c1} \left[\frac{1}{\varepsilon_G} - \frac{1}{\varepsilon_S}\right]\right) + \frac{\tilde{c}_2}{K_2} \exp\left(-y - \hat{u}_{c2} \left[\frac{1}{\varepsilon_G} - \frac{1}{\varepsilon_S}\right]\right)} \right\} \quad \text{in } \Omega_G. \quad (59)
\end{aligned}$$

The boundary conditions remain unchanged from equations (31a)–(31d).

B. Smooth Model

Following the same procedure and definitions from section IIB, we arrive at the modified ODE

TABLE V. Dimensionless Energy Results Molecular Simulation VS Model Prediction.

GAG	Salt		Donnan Potential	Born Hydration Energy	Cation Binding Energy
Hyaluronan	NaCl	Molecular Simulation[13]	0.17±0.06	0.53±0.2	-1.32±0.2
		Model Prediction	0.175	0.527	-1.316
Hyaluronan	KCl	Molecular Simulation[13]	0.44±0.03	0.46±0.2	-1.46±0.2
		Model Prediction	0.430	0.463	-1.469
Heparin	NaCl	Molecular Simulation[13]	-0.62±0.27	1.62±0.6	-3.35±0.6
		Model Prediction	-0.611	1.621	-3.342
Heparin	KCl	Molecular Simulation[13]	0.96±0.14	1.36±0.5	-4.73±0.5
		Model Prediction	0.946	1.362	-4.730

$$-\varepsilon_1(\hat{x}) \frac{d^2 y}{d\hat{x}^2} - \frac{d\varepsilon_1(\hat{x})}{d\hat{x}} \frac{dy}{d\hat{x}} = \bar{c}_1 \exp\left(-y - \frac{\hat{u}_{c1}}{\varepsilon_1(\hat{x})}\right) + \bar{c}_2 \exp\left(-y - \frac{\hat{u}_{c2}}{\varepsilon_1(\hat{x})}\right) - \bar{a} \exp\left(y - \frac{\hat{u}_a}{\varepsilon_1(\hat{x})}\right) - \frac{\bar{g}(\hat{x})}{1 + (\bar{c}_1/\tilde{K}_1) \exp\left(-y - \frac{\hat{u}_{c1}}{\varepsilon_1(\hat{x})}\right) + (\bar{c}_2/\tilde{K}_2) \exp\left(-y - \frac{\hat{u}_{c2}}{\varepsilon_1(\hat{x})}\right)} \quad \text{in } \Omega, \quad (60)$$

where

$$\bar{a} = \bar{c}_1 \exp\left(\frac{\hat{u}_a - \hat{u}_{c1}}{\varepsilon_S}\right) + \bar{c}_2 \exp\left(\frac{\hat{u}_a - \hat{u}_{c2}}{\varepsilon_S}\right). \quad (61)$$

The boundary conditions remain unchanged from equations (34a)–(34b).

C. A Time-Dependent Model

The ODE model focuses on the steady state solution of the GAG/salt system. A complete mathematical description of the system requires consideration of the transient solution prior to reaching steady state. We lay out a foundation for a time-dependent model that we can build on and continue to develop. We begin by assuming a constant permittivity allowing us to neglect the Born energy term for the time being.

For a species, $[C_i]$, undergoing diffusion, chemical reaction, and drift due to an external force, the conservation equation is

$$\frac{\partial [C_i]}{\partial t} + \frac{\partial J_i}{\partial x} = r_i, \quad (62)$$

where r_i is the net rate of production of the ion species per unit volume. Flux J_i depends on the drift velocity, $v_{d,i}$ and the diffusion coefficient, D_i , by

$$J_i = v_{d,i} [C_i] - D_i \frac{\partial [C_i]}{\partial x}. \quad (63)$$

The drift velocity is related to the external force on the species via the mobility, which by the Stokes-Einstein relation is

$$v_{d,i} = \frac{D_i}{k_B T} F_i. \quad (64)$$

Here, the external force, F_i , represents the Coulombic force that drives ion electrophoresis and is proportional to the electric field. Using equation (2) this force can be written

$$F_i = -z_i e \frac{\partial \phi}{\partial x}. \quad (65)$$

Combining equations (62)–(65) yields

$$\frac{\partial [C_i]}{\partial t} + \frac{\partial}{\partial x} \left(-D_i \frac{\partial [C_i]}{\partial x} - \frac{z_i e}{k_B T} D_i \frac{\partial \phi}{\partial x} [C_i] \right) = r_i. \quad (66)$$

To obtain a dimensionless form, we use the same scaling parameters defined previously for concentration, length, and potential. Scale all diffusion constants with some value, D_0 , and define the dimensionless diffusion constants as

$$d_i = \frac{D_i}{D_0}. \quad (67)$$

We can then define a time scale using λ_D and D_0 to obtain

$$\hat{t} = \frac{t}{(\lambda_D^2/D_0)}. \quad (68)$$

Finally, the net rate of production is non-dimensionalized as

$$\hat{r}_i = \frac{\lambda_D^2}{D_0 C_0} r_i. \quad (69)$$

This yields the dimensionless PDE

$$\frac{\partial c_i}{\partial \hat{t}} + \frac{\partial}{\partial \hat{x}} \left(-d_i \frac{\partial c_i}{\partial \hat{x}} - z_i d_i \frac{\partial y}{\partial \hat{x}} c_i \right) = \hat{r}_i. \quad (70)$$

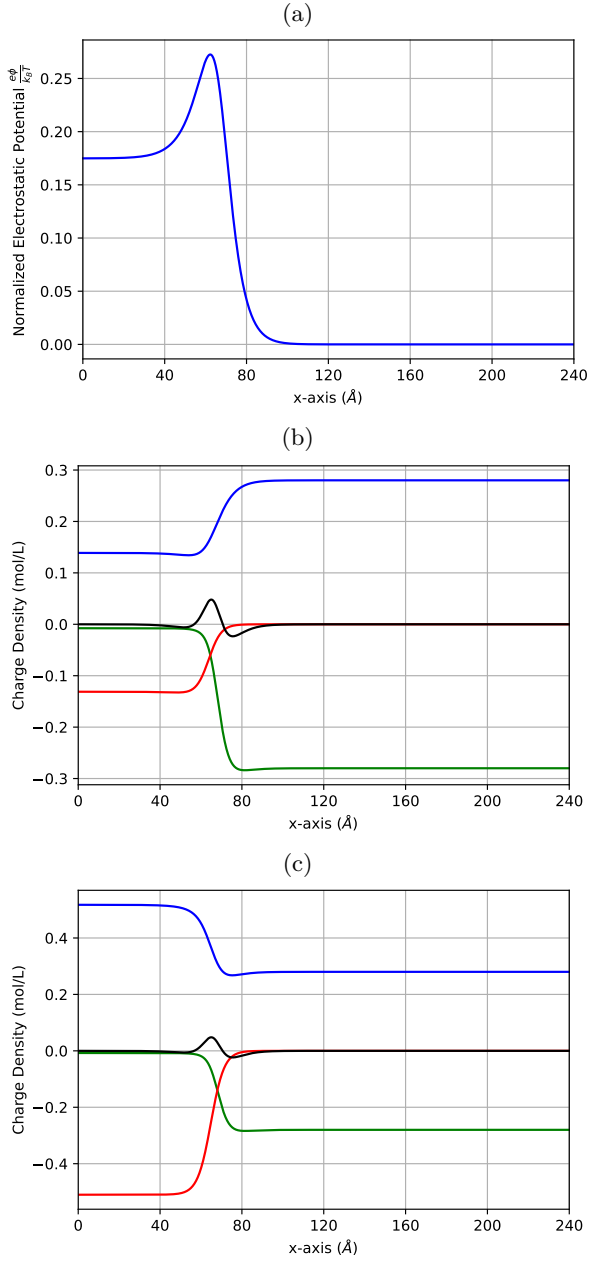


FIG. 4. Hyaluronan NaCl Results. (a) Dimensionless Potential, (b) Unbound Charge Density (M), and (c) Total Charge Density (M) using parameters from Table IV. In (b) and (c), the blue curve represents Na, the green curve represents Cl, the red curve represents Hyaluronan, and the black curve represents the net charge density.

Considering the negatively charged GAG brush in a salt solution consisting of two cations and one anion, the equation for the potential is the same as equation (55) with the ordinary derivatives replaced with partial derivatives and non-dimensionalized as before to obtain

$$-\frac{\partial^2 y}{\partial \hat{x}^2} = c_1 + c_2 - a - g. \quad (71)$$

In this system, the net rates of production are governed

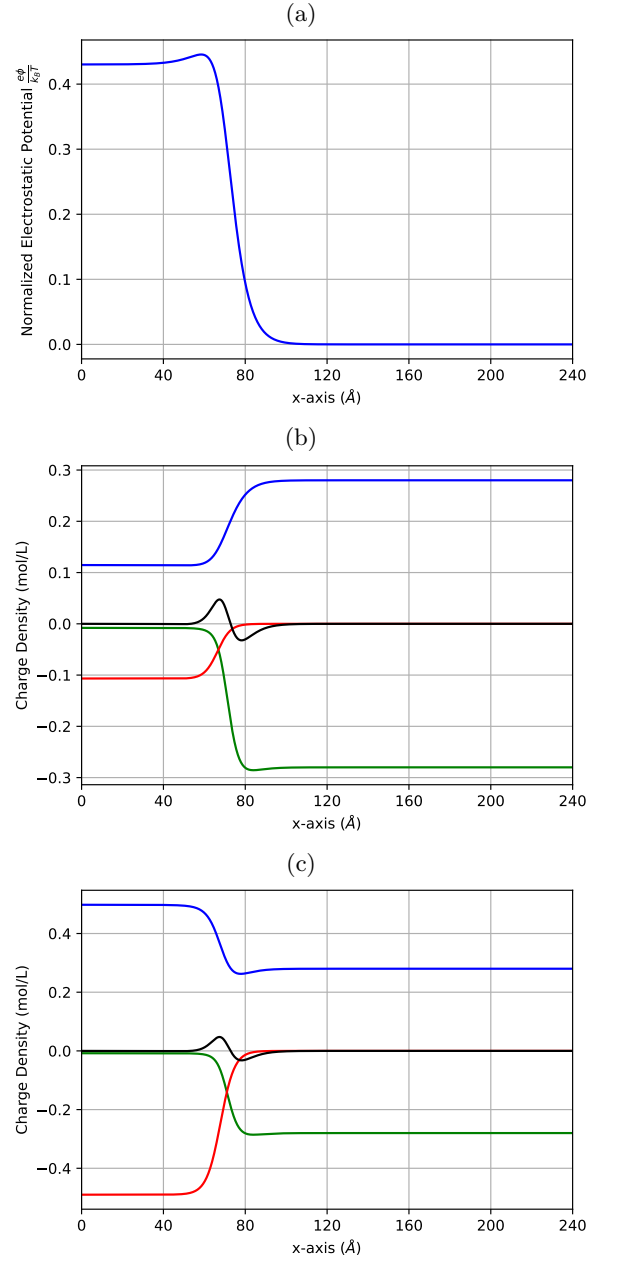
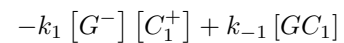
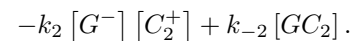


FIG. 5. Hyaluronan KCl Results. (a) Dimensionless Potential, (b) Unbound Charge Density (M), and (c) Total Charge Density (M) using parameters from Table IV. In (b) and (c), the blue curve represents K, the green curve represents Cl, the red curve represents Hyaluronan, and the black curve represents the net charge density.

by the binding chemical reactions



and



The forward reaction rate constants, k_1 and k_2 , can be

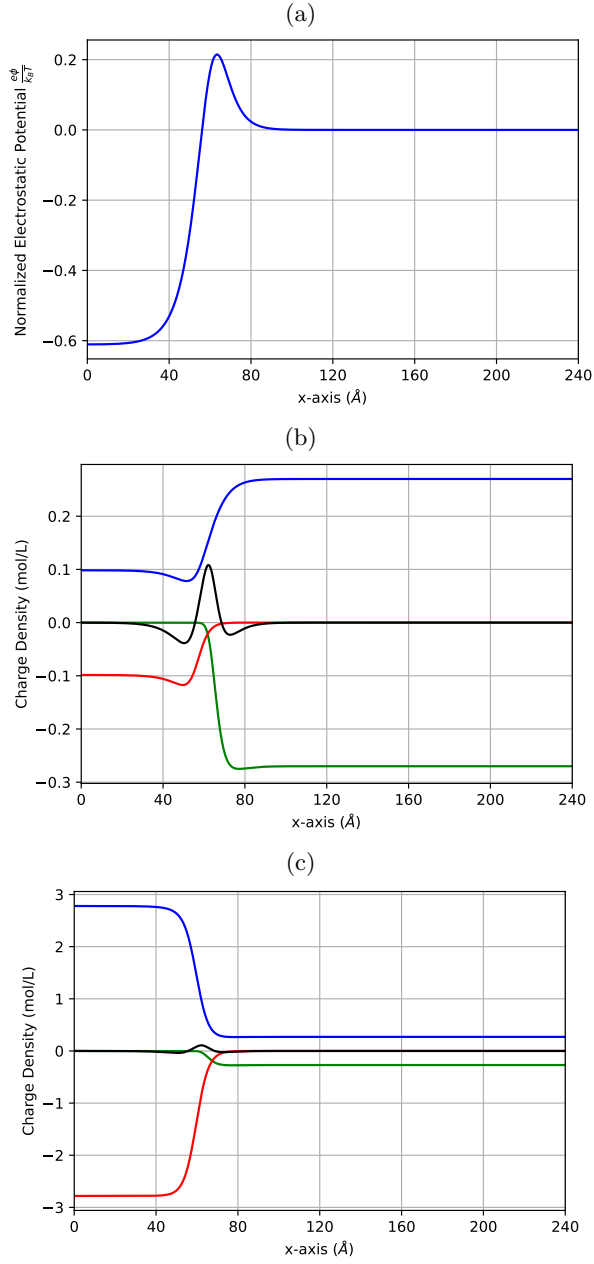


FIG. 6. Heparin NaCl Results. (a) Dimensionless Potential, (b) Unbound Charge Density (M), and (c) Total Charge Density (M) using parameters from Table IV. In (b) and (c), the blue curve represents Na, the green curve represents Cl, the red curve represents Heparin, and the black curve represents the net charge density.

non-dimensionalized as

$$\hat{k}_1 = \frac{\lambda_D^2 C_0}{D_0} k_1, \quad (72a)$$

$$\hat{k}_2 = \frac{\lambda_D^2 C_0}{D_0} k_2. \quad (72b)$$

The backward reaction rate constants, k_{-1} and k_{-2} , can

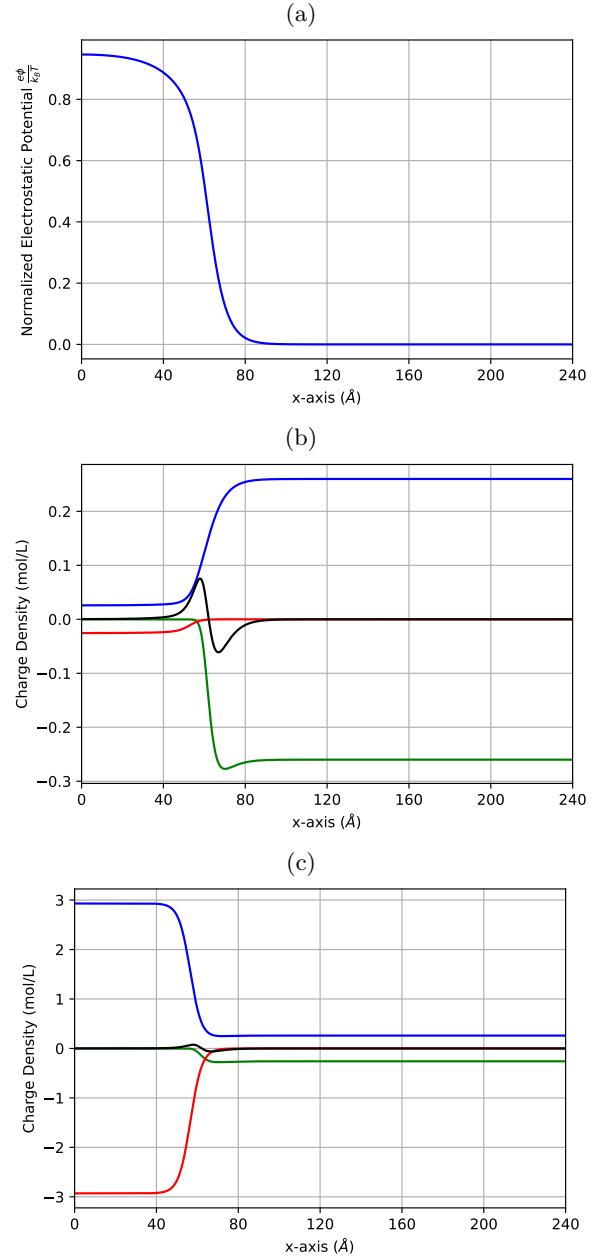


FIG. 7. Heparin KCl Results. (a) Dimensionless Potential, (b) Unbound Charge Density (M), and (c) Total Charge Density (M) using parameters from Table IV. In (b) and (c), the blue curve represents K, the green curve represents Cl, the red curve represents Heparin, and the black curve represents the net charge density.

be non-dimensionalized as

$$\hat{k}_{-1} = \frac{\lambda_D^2}{D_0} k_{-1}, \quad (73a)$$

$$\hat{k}_{-2} = \frac{\lambda_D^2}{D_0} k_{-2}. \quad (73b)$$

Combined with the dimensionless Poisson equation for

the electrostatic potential (71), the dimensionless time-dependent species conservation equations are known as the Poisson-Nernst-Planck (PNP) equations,

$$\frac{\partial c_1}{\partial \hat{t}} + \frac{\partial}{\partial \hat{x}} \left(-d_{c1} \frac{\partial c_1}{\partial \hat{x}} - d_{c1} \frac{\partial y}{\partial \hat{x}} c_1 \right) = -\hat{k}_1 c_1 g + \hat{k}_{-1} [gc_1], \quad (74a)$$

$$\frac{\partial c_2}{\partial \hat{t}} + \frac{\partial}{\partial \hat{x}} \left(-d_{c2} \frac{\partial c_2}{\partial \hat{x}} - d_{c2} \frac{\partial y}{\partial \hat{x}} c_2 \right) = -\hat{k}_2 c_2 g + \hat{k}_{-2} [gc_2], \quad (74b)$$

$$\frac{\partial a}{\partial \hat{t}} + \frac{\partial}{\partial \hat{x}} \left(-d_a \frac{\partial a}{\partial \hat{x}} + d_a \frac{\partial y}{\partial \hat{x}} a \right) = 0, \quad (74c)$$

$$\frac{\partial g}{\partial \hat{t}} = -\hat{k}_1 c_1 g + \hat{k}_{-1} [gc_1] - \hat{k}_2 c_2 g + \hat{k}_{-2} [gc_2], \quad (74d)$$

$$\frac{\partial [gc_1]}{\partial \hat{t}} = \hat{k}_1 c_1 g - \hat{k}_{-1} [gc_1], \quad (74e)$$

$$\frac{\partial [gc_2]}{\partial \hat{t}} = \hat{k}_2 c_2 g - \hat{k}_{-2} [gc_2]. \quad (74f)$$

If there are no surface charge densities on either boundary and no sources or sinks for the cations or anions, then the boundary conditions for all of the dependent variables are homogeneous Neumann boundary conditions.

D. Transient Results

At this point, we want to examine a few example scenarios, look at any interesting transient responses and compare the steady state solution of the time-dependent model to the ODE model. To that end, we defined three different sets of initial conditions shown in Table VI along with Neumann boundary conditions and utilized COMSOL Multiphysics 6.0 to calculate the numerical solutions to our time-dependent model. To keep consistent with our ODE model definitions, we define the GAG brush region to be $0 \leq \hat{x} \leq 10$ and the salt region to be $10 \leq \hat{x} \leq 20$.

We found that the dimensionless unbound cation 2 concentration for scenario 1 had the most interesting transient response. From Table VI, we chose an initial condition for cation 2 such that there was no initial concentration in the GAG brush region and a uniform concentration in the salt region. As seen in Figure 9, unbound cation 2 ions want to leave the salt region and bind with the GAG ions in the brush region. During the transient period, the curve changes from being convex in the brush region and concave in the salt region to being concave in the brush region and convex in the salt region.

The initial condition for all 3 scenarios were chosen in such a way that the steady state solutions should all converge to the same final equilibria. This was achieved by

TABLE VI. Input Parameters and Initial Conditions for the Time-Dependent Model.

Parameter/ Initial Condition	Scenario 1	Scenario 2	Scenario 3
d_{c1}	1	1	1
d_{c2}	1	1	1
d_a	1	1	1
\hat{k}_1	0.5	0.5	0.5
\hat{k}_{-1}	5	5	5
\hat{k}_2	0.5	0.5	0.5
\hat{k}_{-2}	0.5	0.5	0.5
$y(\hat{x}, 0)$	0	see Fig 8	see Fig 8
$c_1(\hat{x}, 0)$	$5 * (\hat{x} < 10)$	see Fig 8	see Fig 8
$c_2(\hat{x}, 0)$	$(\hat{x} > 10)$	$10 * (\hat{x} < 1)$	$10 * (\hat{x} > 19)$
$a(\hat{x}, 0)$	$(\hat{x} > 10)$	$10 * (\hat{x} < 1)$	$10 * (\hat{x} > 19)$
$g(\hat{x}, 0)$	$5 * (\hat{x} < 10)$	see Fig 8	see Fig 8
$[gc_1](\hat{x}, 0)$	0	see Fig 8	see Fig 8
$[gc_2](\hat{x}, 0)$	0	0	0

TABLE VII. Steady State Result Comparison at $\hat{t} = 400$.

Parameter	Scenario 1	Scenario 2	Scenario 3
$y(0, 400)$	-1.41	-1.41	-1.42
$y(20, 400)$	0	0	0
$c_1(0, 400)$	3.21	3.20	3.21
$c_1(20, 400)$	0.78	0.78	0.77
$c_2(0, 400)$	0.23	0.23	0.22
$c_2(20, 400)$	0.055	0.056	0.054
$a(0, 400)$	0.20	0.21	0.20
$a(20, 400)$	0.84	0.84	0.83
$g(0, 400)$	3.23	3.23	3.24
$g(20, 400)$	0	0	0
$[gc_1](0, 400)$	1.04	1.03	1.04
$[gc_1](20, 400)$	0	0	0
$[gc_2](0, 400)$	0.73	0.74	0.72
$[gc_2](20, 400)$	0	0	0

using the same total amount of concentration for each ion when integrated over the whole domain. Table VII shows the boundary values of all the independent variables at $\hat{t} = 400$, which was chosen large enough to allow the system to reach steady state. There is good numerical agreement between the 3 scenarios. This result gives us confidence that the steady state solution is numerically stable.

Using the results in Table VII, we derived the necessary input parameters for our ODE model in Table VIII. The results from our ODE model are overlaid with the results of the 3 scenarios from our time-dependent model in Figure 10.

There is excellent agreement in the steady state solution between our ODE model and the 3 scenarios performed with the time-dependent model. There is a slight artifact that can be seen in the GAG related charge density curves at $\hat{x} = 10$ in the time-dependent model solutions that is due to the step function used for the boundary between the GAG and salt regions. This is

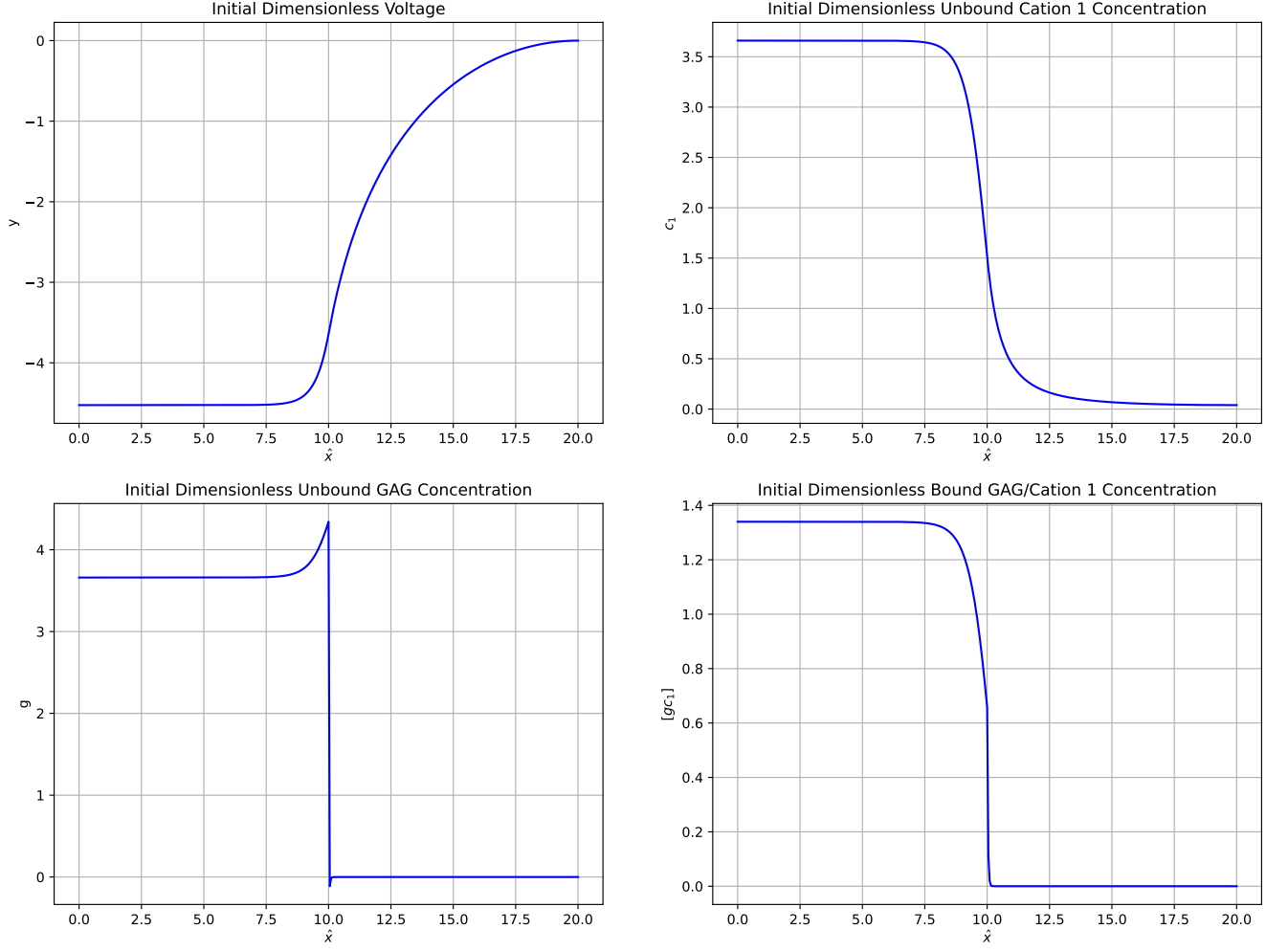


FIG. 8. Initials conditions for voltage (top left), unbound cation 1 concentration (top right), unbound GAG concentration (bottom left), and bound GAG/cation 1 concentration (bottom right).

TABLE VIII. ODE Mode Input Parameters Derived from Time-Dependent Model Steady State Solution.

Parameters	Volume Model
$\hat{\ell}$	10
\hat{L}	20
\tilde{K}_1	10
\tilde{c}_1	0.78
\tilde{K}_2	1
\tilde{c}_2	0.055
\tilde{g}	5
$\hat{\sigma}_1$	0
$\hat{\sigma}_2$	0

strictly numerical in nature and can be resolved by using a smoothed step function. Figure 10 also includes a plot of the dimensionless net charge density, which is the right-hand side of equation (71) at steady state. Using this, we can define a dimensionless net Coulombic force

density as

$$f = -(c_1 + c_2 - a - g) \frac{\partial y}{\partial x}, \quad (75)$$

which is the dimensionless net charge density multiplied by the spatial derivative of the dimensionless potential. We see that both the net charge density and the net force density are zero everywhere except in a region near the boundary between the GAG and salt regions at $\hat{x} = 10$. From the force density, we see that there is a *pinching* effect at the boundary where the force in the GAG region at the boundary is towards the right (salt region) and the force in the salt region at the boundary is towards the left (GAG region). Such a force calculation is more complicated if there is an overshoot in potential as seen in Figures 4 and 6 for GAG brushes with a sodium cation. In these cases, the Coulombic force traversing the brush edge will be right-left-right-left and Born hydration forces also need to be considered in the force balance.

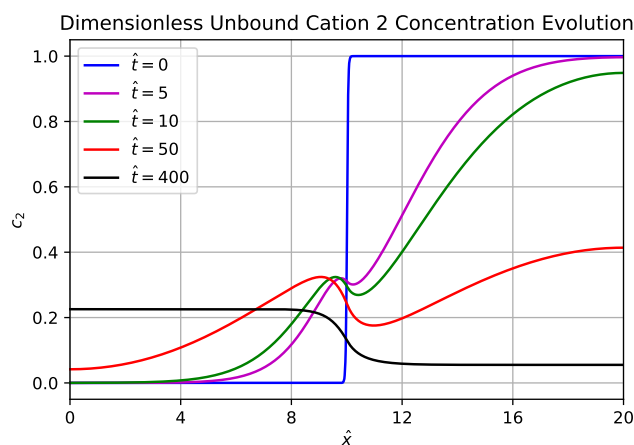


FIG. 9. Time evolution for the dimensionless unbound cation 2 concentration.

VI. CONCLUSION

We have developed steady-state and transient mean-field models for GAG brushes that capture ion-partitioning, ion-pairing, and dielectric decrement effects in GAG brushes. Our models build upon previous Poisson-Boltzmann models [12, 18] and generate the same predicted performance when applying our model in the appropriate limits. We have also shown that our model predictions agree well with the molecular simulation data [13], however our model requires the anion Born radius to be much smaller than typical values found in the literature [17]. The requirement that this unrealistic, nonphysical ion hydration radius be used to match

experimental or molecular dynamics simulation data appears to be a known challenge for Poisson-Boltzmann based models [19]. Furthermore, there is evidence from neutron diffraction experiments on concentrated salt solutions that the chloride ion disrupts the hydrogen-bond network of bulk water much less than the cations; effects that are not captured using the Born hydration formulation implemented herein [20]. Another explanation is that there are additional energy terms such as GAG dipole effects that our model is neglecting. Further research is needed in this area.

Our time-dependent PNP models are shown to be stable and to relax to the PB models, meaning that the imposed jump conditions result in interface profiles that occur at steady-state. Deviations from the steady state profiles that conserve species are shown to relax to the appropriate steady-state.

While we have presented a model where the permittivity is a simple function of x , others have proposed a dependence of the permittivity on ion concentrations [15, 21]. Future work will entail exploring the appropriate relationship between permittivity and ion concentration and incorporating this type of relationship into our model. We will also continue the development of our time-dependent model by incorporating time varying permittivity, the Born energy, and additional energy terms as mentioned above.

The models presented here offer biophysical detail of biological environments that have anionic beds of macromolecules that attain electroneutrality via atomic cations and cationic residues of proteins. The extent to which such biophysical detail can be used to develop new diagnostics, drug-delivery platforms, or therapeutics remains to be seen.

-
- [1] P. De Gennes, *Advances in colloid and interface science* **27**, 189 (1987).
- [2] M. Ballauff and O. Borisov, *Current Opinion in Colloid & Interface Science* **11**, 316 (2006).
- [3] J. Yu, N. E. Jackson, X. Xu, B. K. Brettmann, M. Ruths, J. J. De Pablo, and M. Tirrell, *Science advances* **3**, eaao1497 (2017).
- [4] R. Zimmermann, J. F. Duval, C. Werner, and J. D. Sterling, *Current Opinion in Colloid & Interface Science*, 101590 (2022).
- [5] S. F. Shimobayashi, P. Ronceray, D. W. Sanders, M. P. Haataja, and C. P. Brangwynne, *Nature* **599**, 503 (2021).
- [6] S. Xue, F. Zhou, T. Zhao, H. Zhao, X. Wang, L. Chen, J.-p. Li, and S.-Z. Luo, *Nature communications* **13**, 1 (2022).
- [7] E. Astoricchio, C. Alfano, L. Rajendran, P. A. Temussi, and A. Pastore, *Trends in biochemical sciences* **45**, 706 (2020).
- [8] C. E. Sing and S. L. Perry, *Soft Matter* **16**, 2885 (2020).
- [9] J. T. Granados-Riveron and G. Aquino-Jarquin, *Biomedicine & Pharmacotherapy* **142**, 111953 (2021).
- [10] V. P. Narayanaswamy, L. L. Keagy, K. Duris, W. Wiesmann, A. J. Loughran, S. M. Townsend, and S. Baker, *Frontiers in Microbiology*, 1724 (2018).
- [11] A. B. Edwards, F. L. Mastaglia, N. W. Knuckey, and B. P. Meloni, *Drug Safety* **43**, 957 (2020).
- [12] D. Dean, J. Seog, C. Ortiz, and A. J. Grodzinsky, *Langmuir* **19**, 5526 (2003).
- [13] J. D. Sterling, W. Jiang, W. M. Botello-Smith, and Y. L. Luo, *The Journal of Physical Chemistry B* **125**, 2771 (2021).
- [14] M. Born, *Zeitschrift fur Physik* **1**, 45 (1920).
- [15] J. López-García, J. Horno, and C. Grosse, *Advances in Materials Science and Engineering* **2018** (2018).
- [16] Z.-G. Wang, *Physical Review E* **81**, 021501 (2010).
- [17] L. Sun, X. Liang, N. v. Solms, and G. M. Kontogeorgis, *Industrial & Engineering Chemistry Research* **59**, 11790 (2020).
- [18] J. D. Sterling and S. M. Baker, *Colloids and interface science communications* **100**, 9 (2017).
- [19] B. B. Eakins, S. D. Patel, A. P. Kalra, V. Rezania, K. Shankar, and J. A. Tuszynski, *Frontiers in molecular biosciences* **8** (2021).
- [20] R. Mancinelli, A. Botti, F. Bruni, M. Ricci, and A. Soper,

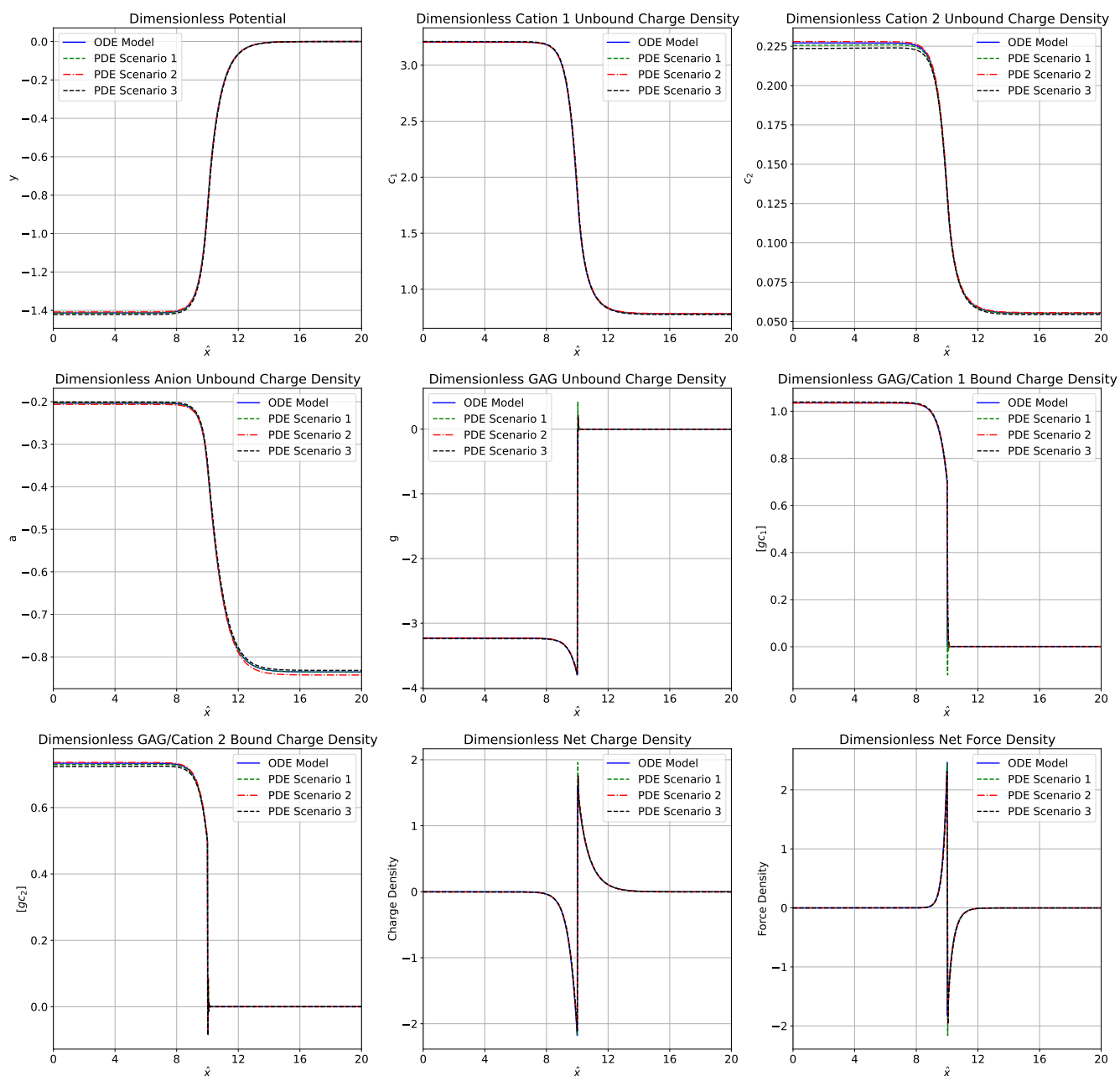


FIG. 10. Overlay of numerical results from ODE model and 3 scenarios performed for the time-dependent model.

The Journal of Physical Chemistry B **111**, 13570 (2007). [21] N. Gavish and K. Promislow, Physical review E **94**, 012611 (2016).